Polarimetric optical-fibre sensor for biochemical measurements

Rene G. Heideman, Rob P. H. Kooyman and Jan Greve

University of Twente, Department of Applied Physics, Applied Optics Group, MESA Research Institute, P.O. Box 217, 7500 AE, Enschede (Netherlands)

(Received July 30, 1992; in revised form December 12, 1992; accepted December 20, 1992)

Abstract

The use of an optical-fibre polarimeter as a chemical sensor is demonstrated. The compound to be detected is allowed to adsorb onto a decladded 5 cm length of the fibre. The fibre is polarization maintaining with an elliptical fibre core and a D-shaped geometry. The overall retardation stability of this fibre polarimeter is $\approx 0.5 \times 2\pi$ rad m^{-1} K^{-1}. With this sensor adsorption processes of proteins can be followed on-line. The resulting relative phase retardations caused by the growth of a monolayer of antibodies (αhCG, αhSA) are $\simeq 0.25 \times 2\pi$. For the much smaller protein hSA, this value is $\cong 0.1 \times 2\pi$.

1. Introduction

The use of optical fibres has received considerable attention in the field of biochemical sensors, especially because of possible *in vivo* use [1]. A fibre-optic device is safe, uses no electrical connection to the body, and is very flexible, so application in a catheter is one of the possibilities.

In most of the fibre-optic biochemical sensors used nowadays, the fibre is only used as a lightguide from source to sensing element, which is attached at the fibre end [2]. A more effective use of the fibre is obtained by using the fibre itself as the sensing element. This can be achieved by exploiting the evanescent field of the light propagating through the fibre. The high intrinsic sensitivity of such a device was demonstrated in a fibre fluorescence immunosensor [3, 4].

Here we want to discuss another type of evanescent-field fibre immunosensor, where no external label molecules are required. The sensor consists of a polarization-maintaining optical fibre that is integrated in a polarimetric detection scheme.

2. Principle of operation

The propagation velocity of light travelling through an optical waveguide is a function of the refractive-index profile surrounding the waveguide core up to a distance of approximately half a wavelength, i.e., the penetration depth of the evanescent field. As a result, any event taking place in the evanescent volume of the waveguide that changes the refractive-index profile causes the propagation velocity to change. We have previously demonstrated that optical interferometry is a potentially very sensitive method to detect very small refractive-index changes in the immediate vicinity of the waveguide surface [5]. Moreover, we have demonstrated that this principle could be applied in a prototype planar waveguide immunosensor [6].

In conventional (fibre) interferometers the two arms of the interferometer are spatially separated. Consider now a fibre with cross section as indicated in Fig. 1, through which two orthogonally polarized modes can propagate (even and odd LP_{01} mode). The elliptical core causes the propagation velocities of these two modes to be slightly different. Generally, this linear birefringence of the fibre transforms input linearly polarized light into elliptically polarized light at the fibre output. By etching away part of the cladding, access is made to the evanescent field region. A changing refractive-index profile near the surface can now modulate the propagation constants of the different modes. At

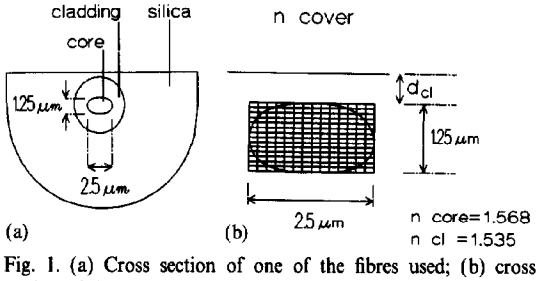

Fig. 1. (a) Cross section of one of the fibres used; (b) cross section of the waveguide structure used in the sensitivity calculations.

0925-4005/93/$6.00

the flat side of the D-shaped fibre the penetration depths, and therefore the sensitivity to changes in the refractive-index profile of the two modes, are slightly different. Consequently, a biochemical surface process modulates the polarization state of the light leaving the fibre.

This polarimetric fibre sensor can be considered as a differential fibre interferometer. Both the reference and the signal arms are contained in the same fibre, resulting in a very simple device. For the fibre polarimeter we expect a reduced sensitivity to environmental drift parameters such as temperature and vibrations when compared to a conventional fibre interferometer [7–9]. The trade-off is, however, that the sensitivity to changes in the refractive-index profile will also be significantly lower.

3. Sensitivity calculations

The D-shaped birefringent fibres used in our experiments are commercially available (Andrew Corporation, IL, USA). The D-shaped geometry of the fibre has two advantages. First, the evanescent-field region of the two modes can be reached by removing only a few micrometres of the surrounding cladding layer, preventing the fibre from becoming very fragile. Secondly, the D-shaped geometry transforms an isotropic removal of the cladding layer into an anisotropic approach of the evanescent fields. The resulting geometrical net difference in overlap of the evanescent fields, and therefore the biochemical sensitivity of the device, can now be optimized.

It should be mentioned that the sensitivity of the individual modes for biochemical surface reactions strongly depends upon two fibre parameters: the refractive-index difference between the core and the cladding, and the core dimensions. For the similar planar waveguide situation it can be calculated [10–12] that this modal biochemical sensitivity increases with increasing refractive-index difference between the core and the cladding. Increasing the core diameter from the cut-off thickness results in a steep increase in sensitivity; however, above a certain optimal thickness the sensitivity gradually drops to zero [12, 13]. The optimal thickness is slightly different for the two orthogonally polarized modes [13]. For the polarimeter sensitivity, i.e., the difference between the two modal sensitivities, this means that its magnitude steeply drops to zero and changes sign, then reaches an extreme value and gradually increases to zero, with increasing core diameter from cut-off thickness [11]. It can be calculated that the polarimeter sensitivity of the fibres used in our experiments is in the gradually increasing part of the sensitivity curve.

TABLE 1. Characteristics of the D-shaped elliptical-core fibres used

Characteristic	Value	
	Fibre 1	Fibre 2
Fibre diameter (μm)	80	80
Jacket diameter (μm)	120	120
Core ellipse (μm)	1.25 × 2.5	1.5 × 3.0
Birefringence B	4×10^{-4}	4×10^{-4}
Refractive-index difference core–cladding	0.033	0.037
Numerical aperture (NA)	0.30–0.34	0.30–0.34
Polarization holding (dB m)	48	45
Attenuation (dB/km)	10 at 0.85 μm	18 at 0.78 μm

Contrary to the analogous planar situation [11, 12], the waveguide parameters of optical fibres cannot easily be optimized. Therefore we shall limit the polarimeter sensitivity calculations to the dependency on accessible parameters.

We have used two different fibres, both single mode for $\lambda = 780$ nm, but with slightly different parameters. The most important characteristics of the fibres used are summarized in Table 1.

The cross section of fibre 1 is schematically drawn in Fig. 1(a). The structure used in the sensitivity calculations is shown in Fig. 1(b). Here the refractive indices of the core and the cladding are calculated for the average value (0.32) of the numerical apertures given in Table 1. The refractive-index values used in the calculations are larger than the actual ones (Andrew Corporation, personal communications). However, as mentioned, the sensitivity of the fibre does not depend strongly on these absolute values, but more upon the difference in refractive index and upon the dimensions of the core. In fact the overall uncertainty in the sensitivity calculations, which will be given in the equations, will always be less than ±25%. This uncertainty arises from the difference between the two fibres used and the absolute refractive-index uncertainty.

For the relative phase retardation $\Delta\Phi$ caused by any process to be monitored, the following formula is used:

$$\Delta\Phi = \Delta B L k_0 = \Delta B L \frac{2\pi}{\lambda_0} \quad \text{(rad)} \tag{1}$$

Here, λ_0 is the wavelength of the laser light used, L the interaction length, and ΔB the change of birefringence caused by the process to be monitored.

3.1. (Biochemical) sensitivity

The biochemical sensitivity of the polarimeter depends upon the difference in penetration depth of the evanescent fields of the two modes at the flat side of the D-shape. The extent of the biochemical response thus

depends upon the thickness of the cladding layer at this side. It is obvious that the protective silica layer and (part of) the cladding layer have to be removed in order to have any penetration of the evanescent field at all.

Several methods are known to calculate numerically the characteristics of a fibre with an elliptical fibre core and asymmetrical D-shaped geometry. The domain integral method (DIM) [14] is very useful because of its ability to calculate the polarimeter sensitivity as a function of cladding thickness. In the DIM a waveguiding region which is embedded in a layered structure is regarded as a perturbation of the background. With a domain-integral equation for the electrical field, the waveguiding parameters can be calculated. The waveguiding region itself can be discretized in a number of subdomains. In our situation a rectangle consisting of the elliptical fibre core and part of the cladding region is divided into 392 small rectangles (see Fig. 1(b)). The elliptical fibre core shape is approximated by filling it up with these small rectangles, yielding a sufficient accuracy.

The birefringence arising from the elliptical geometry, defined as the difference between the effective refractive indices of the LP_{11x} and the LP_{11y} modes, can now be calculated with the DIM. For the unetched fibres it follows that

$$B_{\text{geometry}} = B_g \cong (2.0 \pm 0.1) \times 10^{-4}$$

This value is in perfect agreement with the value obtained with perturbation analysis [15], where the elliptical core geometry is approximated by an equivalent rectangular waveguide using a first-order perturbation approach. This method, however, is only applicable in the unetched situation, where there is only a small difference between the refractive index of the core and that of the cladding.

The calculated geometrical birefringence is not in good agreement with the birefringence data provided by the supplier (see Table 1). However, in this supplier's value not only the geometrical birefringence but also the birefringence originating from thermal stress [16, 17] is included. This contribution can be analytically calculated with the following formula [17, 18]:

$$B_{\text{th.stress}} = B_s = \frac{EC(\alpha_{co} - \alpha_{cl})\,\Delta T\left(1 - \dfrac{a_x}{a_y}\right)}{(1-\nu)\left(1 + \dfrac{a_x}{a_y}\right)} \qquad (2)$$

Here E is Young's modulus, C is the stress optical coefficient, ν is Poisson's ratio, α_{co} and α_{cl} are the temperature-expansion coefficients of the core and cladding glasses, respectively, ΔT is the temperature difference between the softening point of the core and cladding glasses and the ambient temperature, and a_x and a_y are the radii of the short and long major axes of the ellipse, respectively.

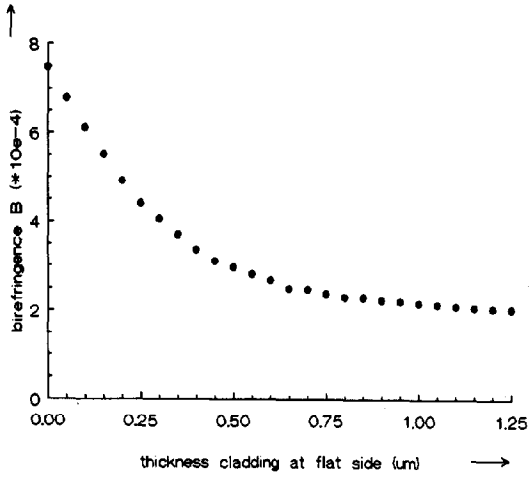

Fig. 2. The resulting ΔB as a function of remaining cladding layer thickness d_{cl}, with $n_{cover} = 1.336$ (water).

In deriving formula (2) it is assumed that E and ν are the same for core and cladding. For E, ν and C, most often the values for fused silica are used, $E \cong 7800$ kg/mm^2 [17], $\nu \cong 0.16$ [16], and $C \cong 3.4 \times 10^{-5}$ mm^2/kg [17–20]. For $(\alpha_{co} - \alpha_{cl})$ we can estimate a value of $\approx 2 \times 10^{-6}$ [16]. With $\Delta T \approx 900$ K, it then follows for the stress-induced birefringence that

$$B_s \cong (1.9 \pm 0.1) \times 10^{-4}$$

The total birefringence is thus in good agreement with the value provided by the supplier. The thermal stress part is not involved in the biochemical sensitivity but determines the temperature dependence. The geometrical part of the normalized birefringence, on the other hand, determines the biochemical sensitivity; its temperature dependence can be neglected.

In Fig. 2 the geometrical birefringence as calculated with the DIM is shown as a function of cladding thickness at the flat side of the D-shape. Here, the refractive index of the cover layer is chosen to be 1.336 (water). From this Figure we see that the normalized birefringence becomes maximal if the cladding is completely removed. Furthermore, it is evident that only at cladding thicknesses below 1 μm does the birefringence significantly deviate from the 'infinite cladding thickness' value, 2×10^{-4}.

The biochemical sensitivity behaviour is calculated in a similar way. We assume adsorption of a monolayer of antibodies, with refractive index 1.45 and thickness 4 nm [21]. The refractive index of the cover layer is chosen to be 1.336, which is the refractive index of a buffer solution (see Section 5) as measured with an Abbe refractometer. The extra birefringence resulting

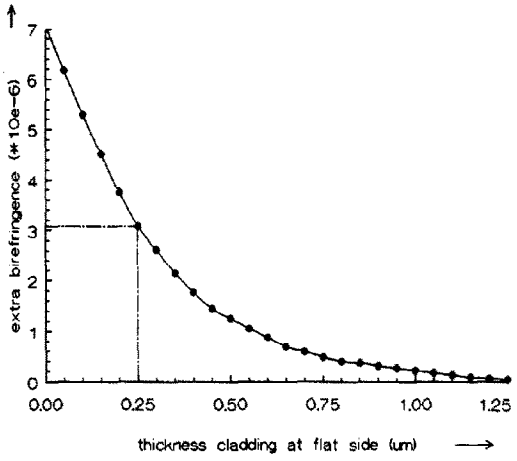

Fig. 3. Calculations of the extra birefringence caused by the growth of a protein monolayer with a thickness of 4 nm and a refractive index of 1.45, as a function of remaining cladding thickness.

from the protein monolayer adsorption is calculated as a function of cladding layer thickness (see Fig. 3).

Not surprisingly, Figs. 2 and 3 exhibit a similar behaviour. From Fig. 3 it is clear that the highest biochemical sensitivity will be achieved when the cladding layer d_{cl} is completely removed. However, as we shall see in Section 5, this situation will be avoided because of the low signal throughput: in practical situations, a balance has to be found between the sensitivity on one hand and the waveguiding quality and strength of the decladded fibre on the other hand. We have found that a reasonable compromise is obtained at a layer thickness $d_{cl} \approx 0.25$ μm. Here, the biochemical sensitivity is half the maximal value.

With $d_{cl} \approx 0.25$ μm and $\lambda_0 = 780$ nm, the bulk refractive-index step from air ($n = 1.00$) to pure water ($n = 1.336$) can be calculated to give rise to a relative phase retardation (see eqn. (1)):

$$\Delta\Phi \cong L(250 \pm 25)2\pi \quad \text{(rad)} \tag{3}$$

From Fig. 3 it follows that complete antibody protein monolayer adsorption results in a relative phase retardation

$$\Delta\Phi \cong L(4 \pm 1)2\pi \quad \text{(rad)} \tag{4}$$

When compared to the sensitivity of a well-designed [5, 13] waveguide structure in a Mach–Zehnder interferometer configuration [12], the difference is enormous. In that situation the same protein monolayer adsorption results in a phase change of $\approx 35 \times 2\pi$, with an interaction length of only 1 cm.

3.2. Temperature dependence

The biochemical sensitivity of the polarimeter is obtained by small deviations from the initial geometry of the refractive-index profile around the fibre, thereby changing the geometrical birefringence. However, the temperature dependence originates from the thermal-stress-induced birefringence of the fibre. For the temperature dependence of the relative phase retardation we can rewrite eqn. (1) as

$$\Delta\Phi = L\left(\frac{2\pi}{\lambda_0}\right)\left(\frac{\partial B_s}{\partial T}\right)\Delta T \quad \text{(rad)} \tag{5}$$

With formula (2) it can easily be calculated that $\partial B_s/\partial T \approx 4 \times 10^{-7}\ \mathrm{K}^{-1}$. Here the temperature effects on E, C, α, ν and a are negligible. For the relative phase retardation it now follows with $\lambda_0 = 780$ nm that

$$\Delta\Phi \cong (0.5 \pm 0.1)L\ \Delta T 2\pi \quad \text{(rad)} \tag{6}$$

This temperature dependence is rather large when compared to the biochemical sensitivity (eqn. (4)) of the polarimeter, and enormous in comparison with that of the planar waveguide interferometer [12]. The big advantage of the fibre polarimeter is not its sensitivity, however, but the very simple design and the flexibility of the fibre.

4. Experimental set-up

The basic configuration of our fibre polarimeter is shown in Fig. 4. A temperature-stabilized single-mode Hitachi HL7806G laser diode (LD) was used as the light source with wavelength 780 nm. The laser light is collimated with a compact disk (CD) lens, travels through a Faraday rotator (IO-D-780, OFR, NJ, USA) and a half-wave plate ($\lambda/2$). It is launched into the polarization-maintaining fibre through a 20 × microscope objective (MO) by using a fibre-optic positioner (FOP). The Faraday rotator (FR) prevents backscattering of laser light into the laser cavity, originating from relections from the two fibre ends and the half-wave plate. In this way mode-hops are avoided, which would otherwise limit the stability of the polarimeter. The half-wave plate is used to launch equal amplitudes of linearly polarized light into both modes of the fibre. In the sensing element (SE), described in the next Section, the polarization state is modulated by a changing chemical environment.

The elliptically polarized output beam is collimated with a microscope objective and passes a Pockels cell (EOD, PC100/4 series). A voltage applied to this cell (PC) changes the difference in refractive index between its two axes and therefore the state of ellipticity of the light passing through. The axes of the Pockels cell are parallel with the axes of the fibre core ellipse. Behind the Pockels cell a polarizing cube beamsplitter (PBS) is placed, with its axes at an angle of 45° to those of the Pockels cell. The intensities of the reflected and transmitted beams are measured with photodiodes (PD).

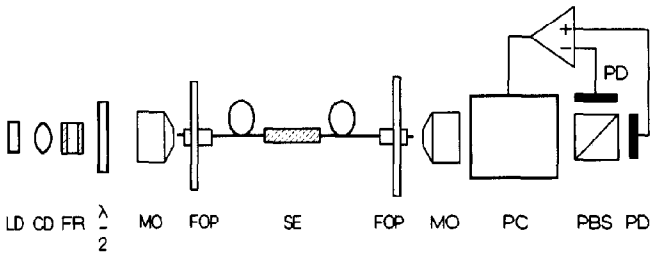

Fig. 4. The basic configuration of the fibre polarimeter. For explanation of the abbreviations, see text.

By regulating the voltage applied to the Pockels cell, the difference between the two measured intensities can be regulated to zero. A feedback loop is used for this. In this situation the initially elliptically polarized fibre output is actively transformed into circularly polarized light. By taking the regulation voltage as the signal, a constant (maximal) sensitivity and a decreased intensity dependence are provided. Furthermore, the applied voltage is proportional to the relative phase retardation caused by the processes to be monitored.

The maximum relative phase retardation that can be introduced on-line with the Pockels cell is limited to $\cong 2\pi$. The resolution is better than $1 \times 10^{-3} \times 2\pi$. The temperature dependence of the Pockels cell is $\approx 0.02 \times 2\pi$ rad K^{-1}. The temperature dependence of the fibre polarimetric response is experimentally found to be much larger, $\approx 0.5 \times 2\pi$ rad m^{-1} K^{-1}. This is in good agreement with the calculated dependence (eqn. (5)).

5. Results and discussion

5.1. Preparation of the fibre sensing element

As indicated in Section 2, it is necessary to remove the complete protective silica layer and part of the cladding layer of the fibre to obtain a biochemically sensitive polarimeter. This is done by wet chemical etching of a certain length (interaction length) of the fibre, yielding the sensing element. The etchant used is a mixture consisting of three liquids; a standard SiO_2 etchant solution with a volume ratio $HF:NH_4F = 12\frac{1}{2}:87\frac{1}{2}$ (ammonium fluoride etchant AF, Merck), distilled water and an NH_4F solution with volume ratio $NH_4F:H_2O \equiv 2:3$ (40% ammonium fluoride solution, Merck). In order to get a well-defined interaction length, an HF-resistant polymer layer (Shipley Microposit photoresist, s1400-31) is deposited on the fibre outside the sensing element. Afterwards, this protective layer can be removed from the fibre using acetone. In our experiments the interaction length is chosen to be (5 ± 0.2) cm because of practical considerations, while the fibre itself is ≈ 30 cm long.

The etching process of the silica layer can be followed on-line using the set-up shown in Fig. 4. During this process the feedback loop is not activated because of the limited range of the Pockels cell. In view of the large relative phase retardations involved, simple fringe counting can be applied. The etching procedure is stopped by removing the fibre from the etchant, after which the fibre is rinsed with pure water.

From the literature it is known that the smoothness of the etched fibre surface is dependent upon the etchant composition [22]. Therefore the etching procedure was performed with three etching liquids. Here the mixture composition of etchant solution was varied. In Fig. 5 the results are summarized. From Fig. 5(a) it is clear that increasing the HF fraction results in higher etching rates and thus in more relative phase retardation per unit time. Etching too fast, however, is concomitant with deteriorating waveguiding characteristics, as seen in Fig. 5(b). The same holds to a lesser extent for etching too slowly. Satisfactory results are obtained with the 'etchant 2', with the composition (volume ratio) standard SiO_2 etchant:H_2O:40% $NH_4F \equiv 1:1:1$. This etchant was used for the further experiments.

From Section 3 it is known that the highest biochemical sensitivity is obtained by completely removing the cladding layer (see Fig. 4). With an interaction length of 5 cm, this is equivalent to the passage of ≈ 25 fringes as observed with a test fibre. As a compromise between signal throughput and fibre strength on the one hand, and sensitivity on the other, the cladding is etched until approximately 12 fringes have passed (see Fig. 5). In view of the maximum number of fringes, it can be calculated that the remaining cladding thickness is $\cong 0.25$ μm (see Fig. 3). This is the d_{cl} value used in Section 3.

5.2. Coating of the fibre surface and immuno experiments

Before the biochemical experiments are started, the sensitivity of the fibre can be checked with bulk refractive-index steps. Hereto the etched part of the fibre is placed in a large PMMA flow-through cuvette, with length 100 mm and diameter 1 cm. With a peristaltic

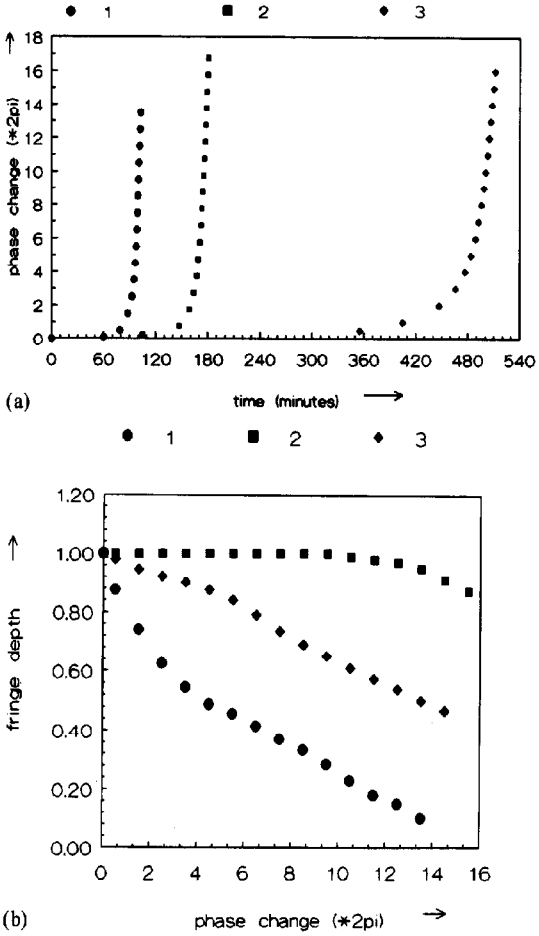

Fig. 5. The etch process of the sensing element, with an interaction length $\cong 5$ cm. The etchant solution is a mixture of three liquids (see text). The volume ratio of standard SiO_2 etchant: H_2O:40% NH_4F solution is used as a parameter: etchant $1 \cong 1{:}0{:}0$; etchant $2 \cong 1{:}0{:}6$; etchant $3 \cong 1{:}1{:}1$. (a) The resulting phase change as a function of time. (b) The resulting fringe depth as a function of phase change.

pump pure water is pumped slowly through the cuvette. The relative phase retardation corresponding to this bulk refractive-index step of 0.334 is $(14 \pm 1) \times 2\pi$ in all cases. This is in good agreement with the calculated value for $L = 5$ cm (see eqn. (3)).

After this sensitivity check the biochemical experiments are started, for which the fibre is placed in a PTFE cuvette. Open (65 mm length × 6 mm width × 4 mm height, content $\cong 2$ ml) as well as flow-through (100 mm length, 2 mm diameter, content $\cong 0.3$ ml) cuvettes were used. The cuvette is then filled with a buffer solution. Both Sörensen buffer (SB, osmolality $= 150 \pm 10$ mOsmol/kg H_2O, pH = 7.40) as well as phosphate buffer solution (PBS, osmolality $= 280 \pm 10$ mOsmol/kg H_2O, pH = 7.35) were used, but no difference in behaviour was found.

From this moment the feedback loop of the Pockels cell is activated. In this way the kinetics of the coating of the receptor molecules onto the fibre surface can be monitored. The coating of the receptor layer is done by adsorption. We have used two different coating procedures as well as different receptor molecule types.

In the first coating procedure, the buffer solution is replaced by a solution containing 0.05 mg/ml protein. This was followed by the immuno experiments, in which the cuvette is filled with a solution containing the specific partner molecule of the adsorbed protein. In all cases we were unable to detect unambiguously the immune reactions. The proteins used for coating are human serum albumin (hSA, molecular weight ≈ 65 kD), the polyclonal antibody anti-human serum albumin (αhSA, molecular weight ≈ 150 kD) and the monoclonal antibody anti-human chorionic gonadotropin (αhCG, molecular weight ≈ 150 kD). In Fig. 6(a) the typical relative phase retardations resulting from the adsorption of these types of protein are shown. The equilibrium values shown in Fig. 6(a) exhibit a reproducibility of $\approx 10\%$. The experimentally found kinetics qualitatively correspond to those for a diffusion-limited adsorption, which is expected for this type of surface reaction.

The added protein concentration was chosen high enough to result in a complete equilibrium monolayer coverage of the fibre surface. This was confirmed by adding even higher concentrations of these proteins, which did not result in further adsorption. The measured equilibrium phase retardations corresponding to the antibody protein monolayers are $\cong 0.22 \times 2\pi$, as can be seen from Fig. 6(a). This value is in good agreement with the estimates made in eqn. (4) for $L = 5 \times 10^{-2}$ m, where a protein monolayer thickness value of 4 nm with refractive index of 1.45 was used.

The difference in molecular weight between the smaller antigen protein hSA and the two larger antibody proteins αhSA and αhCG is reflected in the relative phase retardations corresponding to the respective monolayers. The phase retardation ratio is ≈ 2, which is also measured with the planar waveguide interferometer [12]. This value is in good agreement with the ratio in molecular weights. Assuming the same refractive index, this means an hSA monolayer thickness of ≈ 2 nm.

The second coating procedure is based on earlier communications [12, 23] in which we have indicated that coating of approximately one third of a monolayer on a hydrophobic surface leads to an optimum immunoresponse. However, application of this procedure (see Fig. 6(b)) to the present device does not result in an umambiguous detection of an immunoreaction. We believe that this is due to the fact that the temperature stability of the fibre polarimeter is not sufficient:

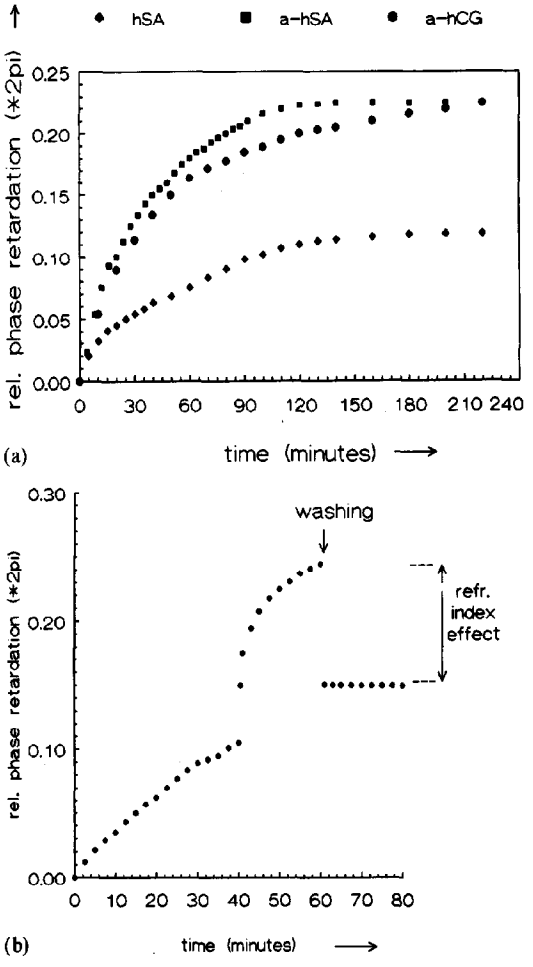

Fig. 6. The relative phase retardation as a function of time caused by the two different coating procedures used. (a) The adsorption of monolayers of three different proteins, starting at $t = 0$ min. (b) The adsorption of a fraction ($\cong 0.3$) of a monolayer of the antibody αhCG, followed by a blocking procedure [19, 21] after 40 min. The blocking procedure is performed with a high concentration of the protein (bSA) in order to prevent non-specific adsorption. Before the adsorption, the fibre was dipped in hexamethyldisilane (HMDS), yielding a hydrophobic fibre surface.

for an optimum antibody coating we expect on the basis of our previous measurements [12, 23] a maximum immunoresponse corresponding to a signal of $\Delta\Phi \cong 0.015 \times 2\pi$, which is comparable to the phase fluctuations originating from a temperature variation of 0.1 K.

6. Conclusions

In this paper we have demonstrated that the growth of a layer of proteins can be sensitively detected using a polarization-maintaining D-shaped fibre in a polarimeter configuration. The interaction length of the prepared fibre is $\cong 5$ cm. The resulting relative phase retardations caused by the growth of a monolayer of antibodies (αhSA, αhCG) are $\cong 0.25 \times 2\pi$. For a monolayer of the much smaller protein hSA this value is $\cong 0.1 \times 2\pi$. These results are in good agreement with the calculated sensitivity of the device for adsorption of a monolayer.

The phase resolution of the present fibre sensor assembly (30 cm fibre length, 5 cm interaction length) for protein ($n = 1.45$) layer growth is $\approx 0.04 \times 2\pi$ rad nm^{-1}. The temperature stability is estimated at $\approx 0.5 \times 2\pi$ rad m^{-1} K^{-1}. In our experiments a temperature rise of 0.1 K thus gives rise to a relative phase retardation of $0.015 \times 2\pi$ rad. This is the same order of magnitude as the maximal immune response to be expected for the receptor-layer coating procedure we have used. With this receptor-layer coating procedure the sensor is obviously not suitable for monitoring immunoreactions. However, with more sophisticated receptor-layer coating procedures the signals arising from immunoreactions can be at least two orders of magnitude increased [24] when compared with a covalently bound receptor-layer situation (which is already better than the adsorption procedure used in our experiments).

The biochemical sensitivity of the fibre polarimeter strongly depends upon the intrinsic fibre parameters (numerical aperture and core diameter) and upon accessible parameters such as the remaining cladding thickness. In the present communication we have only investigated the influence of this last parameter. However, it is obvious that a careful selection of particular intrinsic fibre parameters and an appropriate optical wavelength could significantly increase the overall sensor performance.

The performance of the sensor can also be improved by increasing the interaction length:fibre length ratio. Further considerable improvements can be expected by using a D-shaped fibre in a double mode [25], or even a three-mode option. Here both temperature effects as well as the biochemical surface reactions can in principle be distinguished by using an appropriate detection scheme.

Acknowledgements

These investigations in the programme of the Foundation for Fundamental Research on Matter (FOM) have been supported in part by the Netherlands Technology Foundation (STW).

The domain integral method calculations were performed at the Dr Neher Laboratory, PTT, The Netherlands. We would like to thank Dr N. H. G. Baken for this opportunity.

The authors wish to thank Dave van den Heuvel for the preparation of the protein-containing solutions.

References

1 J. W. Petersen and G. G. Vurek, Fiber-optic sensors for biomedical applications, *Science, 224* (1984) 123–127.
2 M. S. Abdel-Latif, A. Suleiman and G. G. Guilbault, Fiber-optic sensors: recent developments, *Anal. Lett., 23* (1990) 375–399.
3 R. G. Eenink, H. E. de Bruijn, R. P. H. Kooyman and J. Greve, Fibre-fluorescence immunosensor based on evanescent wave detection, *Anal. Chim. Acta, 238* (1990) 317–321.
4 T. R. Glass, S. Lackie and T. Hirschfeld, Effect of numerical aperture on signal level in cylindrical waveguide evanescent fluorosensors, *Appl. Opt., 26* (1987) 2181–2186.
5 R. G. Heideman, R. P. H. Kooyman, J. Greve and B. S. F. Altenburg, Simple interferometer for evanescent field refractive index sensing as a feasibility study for an immunosensor, *Appl. Opt., 30* (1991) 1474–1479.
6 R. G. Heideman, R. P. H. Kooyman and J. Greve, Development of an optical waveguide interferometric immunosensor, *Sensors and Actuators B, 4* (1991) 297–299.
7 F. Maystre and R. Dandliker, Polarimetric fibre optical sensor with high sensitivity using a Fabry–Perot structure, *Appl. Opt., 28* (1989) 1995–2000.
8 A. D. Kersey, M. A. Davis and M. J. Marrone, Differential polarimetric fiber-optic sensor configuration with dual wavelength operation, *Appl. Opt., 28* (1989) 204–206.
9 T. H. Chua and C.-L. Chen, Fiber polarimetric stress sensors, *Appl. Opt., 28* (1989) 3158–3165.
10 Ch. Fattinger, H. Koller and P. Wehrli, The difference interferometer: a highly sensitive probe for molecular surface-coverage detection, *Proc. Biosensors '92, Geneva, Switzerland, 1992*, pp 339–346.
11 W. Lukosz and Ch. Stamm, Integrated optical interferometer as relative humidity sensor and differential refractometer, *Sensors and Actuators A, 25–27* (1991) 185–188.
12 R. G. Heideman, R. P. H. Kooyman and J. Greve, Performance of a highly sensitive Mach–Zehnder interferometer, *Sensors and Actuators B, 10* (1992) 209–217.
13 K. Tiefenthaler and W. Lukosz, Sensitivity of grating couplers as integrated-optical chemical sensors, *J. Opt. Soc. Am. B., 6* (1989) 209–220.
14 N. H. G. Baken, Computational modeling of integrated-optical waveguides, *Dissertation*, University of Delft, The Netherlands, 1990.
15 A. Kumar, R. K. Varshney and K. Thyagarajan, Birefringence calculations in elliptical-core optical fibres, *Electron. Lett., 20* (1989) 112–113.
16 J.-I. Sakai and T. Kimura, Birefringence caused by thermal stress in elliptically deformed core optical fibers, *IEEE J. Quantum Electron., QE-18* (1982) 1899–1909.
17 K. Okamoto, T. Hosaka and T. Edahiro, Stress analysis of optical fibers by a finite element method, *IEEE J. Quantum Electron., QE-17* (1981) 2123–2129.
18 P. L. Chu, Thermal-stress-induced birefringence in single-mode elliptical optical fibre, *Electron. Lett., 18* (1982) 45–47.
19 S. Tammela, P. Koivisto and M. Leppihalme, Fabrication and properties of a single mode waveguide embedded inside the wall of a capillary tubes, *Fiber Optic Sensors 3, SPIE Proc.*, Vol. 1011, 1988, pp. 67–70.
20 N. Imoto, N. Yoshizawa, J.-I. Sakai and H. Tsuchiya, Birefringence in single-mode optical fiber due to elliptical core defor-mation and stress anisotropy, *IEEE J. Quantum Electron., QE-16* (1980) 1267–1271.
21 H. E. de Bruijn, B. S. F. Altenburg, R. P. H. Kooyman and J. Greve, Determination of thickness and dielectric constant of thin transparent dielectric layers using surface plasmon resonance, *Opt. Commun., 82* (1991) 425–432.
22 T. Hosaka, K. Okamoto and J. Noda, Single-mode fibre-type polarizer, *IEEE J. Quantum Electron., QE-18* (1982) 1569–1572.
23 R. G. Heideman, R. P. H. Kooyman and J. Greve, Optical waveguide interferometric immunosensor, *Proc. Biosensors '92, Geneva, Switzerland, 1992*, pp. 356–362.
24 U. Jönsson, Real-time biospecific interaction analysis, *Proc. Biosensors '92, Geneva, Switzerland, 1992*, pp. 260–266.
25 J. N. Blake, S. Y. Huang and B. Y. Kim, Elliptical core two-mode fiber strain gauge, *Fiber Optic and Laser Sensors 5, SPIE Proc.*, Vol. 838, 1987, pp. 332–339.

Biographies

Rene Heideman was born in Goor, The Netherlands in April 1965. He received his degree in applied physics from the University of Twente, The Netherlands, in August 1988. He is presently working towards his Ph.D. degree by developing biochemical sensors based on planar and fibre-optical waveguides.

Rob Kooyman received his M.S. degree in physics at Leiden University in 1975. From 1975 to 1980 he worked at the Agricultural University at Wageningen on a Ph.D. thesis devoted to molecular spectroscopy. At the University of Utrecht he developed spectroscopic methods for use in membrane biophysics. Since 1985 he has been involved in biosensor research at the University of Twente.

Jan Greve was born in Koog aan de Zaan, The Netherlands, on October 24, 1939. He received his M.S. degree in experimental physics from the Free University, Amsterdam, The Netherlands, in 1967 and a Ph.D. degree from the same university in 1972.

Since 1967 he has been working in the field of biophysics, applying and developing macromolecules, bacteriophages and cells. In 1980 Professor Greve started a biophysics subgroup of the opto-electronics group in the Applied Physics Department of the University of Twente. The current research interests of the group are micro-Raman spectroscopy of biological macromolecules, cell characterization, mini-laser Doppler flowmeters and biosensors.